Journal of Biomolecular Structure & Dynamics, ISSN 0739-1102
Volume 17, Issue Number 6, (2000)

Effect of Coordinated Ions on Structure and Flexibility of Parallel G-quadruplexes: A Molecular Dynamics Study

Shibasish Chowdhury and Manju Bansal*
Molecular Biophysics Unit,
Indian Institute of Science,
Bangalore-560012, India

http://www.adeninepress.com

Abstract

Single tract guanine residues can associate to form stable parallel quadruplex structures in the presence of certain cations. Nanosecond scale molecular dynamics simulations have been performed on fully solvated fibre model of parallel d(G_7) quadruplex structures with Na^+ or K^+ ions coordinated in the cavity formed by the O6 atoms of the guanine bases. The AMBER 4.1 force field and Particle Mesh Ewald technique for electrostatic interactions have been used in all simulations. These quadruplex structures are stable during the simulation, with the middle four base tetrads showing root mean square deviation values between 0.5 to 0.8 Å from the initial structure as well the high resolution crystal structure. Even in the absence of any coordinated ion in the initial structure, the G-quadruplex structure remains intact throughout the simulation. During the 1.1 ns MD simulation, one Na^+ counter ion from the solvent as well as several water molecules enter the central cavity to occupy the empty coordination sites within the parallel quadruplex and help stabilize the structure. Hydrogen bonding pattern depends on the nature of the coordinated ion, with the G-tetrad undergoing local structural variation to accommodate cations of different sizes. In the absence of any coordinated ion, due to strong mutual repulsion, O6 atoms within G-tetrad are forced farther apart from each other, which leads to a considerably different hydrogen bonding scheme within the G-tetrads and very favourable interaction energy between the guanine bases constituting a G-tetrad. However, a coordinated ion between G-tetrads provides extra stacking energy for the G-tetrads and makes the quadruplex structure more rigid. Na^+ ions, within the quadruplex cavity, are more mobile than coordinated K^+ ions. A number of hydrogen bonded water molecules are observed within the grooves of all quadruplex structures.

Introduction

The formation of higher order helical structures by contiguous guanine stretches *in vitro,* has been well known for decades (1,2). In recent years, there has been renewed interest in them, since such guanine rich repetitive sequences occur at the eukaryotic chromosomal termini (3-6), immunoglobulin switch regions of higher organisms (7), mutation hotspots associated with human diseases (8),"CpG" islands located in the coding and promoter regions of genes (9), HIV-1 genomic RNA (10) and in triplet repeat sequences associated with fragile X syndrome (11). It is now well established that in presence of alkali cations, guanine rich sequences form four stranded quadruplex structures stabilized by stacked and almost planar guanine quartets (G-tetrad) formed by four Hoogsteen type hydrogen bonded guanine bases as shown in Figure 1 (12,13). Identification of various proteins which can bind guanine rich sequences and facilitate formation of four stranded structures, further supports the presence of G-quadruplex structures *in vivo* (9,14-17). Fibre diffraction studies (18,19) and crystal structures (20,21) clearly demonstrate the formation of four stranded quadruplex structures which are stabilized by stacked guanine tetrads. Cations also play an important role in stabilizing G-

*Phone:+91-80-309-2534;
Fax: +91-80-3600683;
E-mail: mb@mbu.iisc.ernet.in

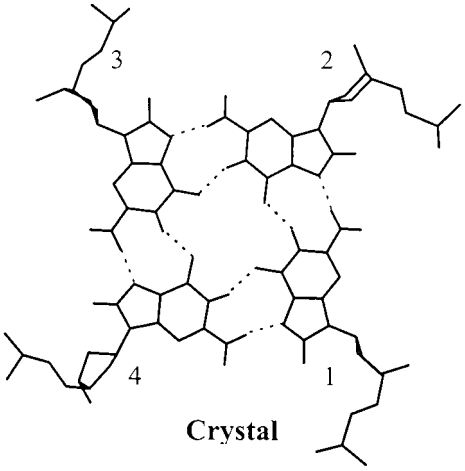

Figure 1: A down the helix axis view of a representative G-tetrad in the parallel stranded all-anti, G-stem in the crystal structure (21) of d(TG_4T) sequence. Dotted lines indicate the hydrogen bonds, for which hydrogen to acceptor atom distance is < 2.6Å. The strand numbering scheme used in all subsequent figures is also shown.

quadruplexes by coordinating eight closely spaced guanine O6 atoms between the planes of neighbouring G-quartets. Recent crystallographic studies have provided definite evidence of such coordination for K^+ ions in dimeric G-quadruplex (20) and Na^+ ions in tetrameric G-quadruplex (21). Conformational polymorphism in guanine quadruplex structures are shown by several theoretical studies (22-27). Oligonucleotides with a single contiguous guanine stretch favour the formation of parallel stranded intermolecular structures (28-33) and multiple non-contiguous guanine stretches can form antiparallel structures either by dimerization of hairpin duplexes (28,33,34,36,37) or by intramolecular folding of a single strand (38-40). Several physicochemical and NMR studies have demonstrated that topology of different quadruplexes depend upon ionic concentration and size of different cations (32,33,41-43). A structural explanation has been proposed for the large differences in the stability of the quadruplex formed by specific cations. The ion which is smaller than the quadruplex cavity, would not bind tightly the keto oxygens of guanines (5) or it may disrupt the quadruplex structure by pulling the oppositely charged O6 atoms into a partially vacant central cavity while larger cation may cause the steric disruption of hydrogen bonds between the strands (44). It is also observed that NMR spectrum of NaCl stabilized quadruplexes differs significantly from KCl stabilized quadruplexes (43,45). NMR and thermodynamic studies demonstrated that if the cations are trapped inside the quadruplex cavity, their binding behavior and dynamic motion are different from externally bound counter ions and the various cations also behave differently (46-49).

We have earlier reported preliminary analysis of nanosecond scale molecular dynamics (MD) simulations on parallel $d(G)_7$ quadruplexes with coordinated Na^+ ions between the G-tetrads and surrounded by explicit water molecules and Na^+ ions (25). In order to understand the effect of coordinated cation on the quadruplex geometry, MD was also performed on a parallel quadruplex without any coordinated ion and it was found that the structure remains intact during the simulation. A recent detailed study on $d(G)_4$ quadruplex structures reported similar results for the Na^+ ion coordinated structures, but the 4-mer without any coordinated ion was found to undergo partial disassociation and strand slippage (27). Here we report a detailed analysis of parallel quadruplex structures, with Na^+ and K^+ coordinated ions as well as without ions, with particular emphasis on the effect of coordinated ion on hydrogen bond patterns in the G-tetrads and tetrad stacking energy, as well as hydration in the well defined grooves of the 7-mer quadruplexes. It was found that, while the G-quadruplex structure without any coordinated ion is intrinsically more flexible, favourable DNA-coordinated ion interaction makes these structures more rigid. Furthermore, the smaller Na^+ ion fits into the quadruplex cavity more easily than a K^+ ion. However, lifetime of a Na^+ ion in the coordinated site is shorter than that for a K^+ ion, since it is more mobile within the cavity.

Methods

The initial 7-mer quadruplex structure of poly d(G) with all four chains in parallel orientation was generated using the parameters from the fibre diffraction model of poly-rI (18) since it has a C2′-*endo* sugar pucker and is therefore more representative of a DNA quadruplex structure than the C3′-*endo* model for poly-rG (19). Six K^+ or Na^+ ions were placed between the seven G-tetrads, as observed in the x-ray crystal structure (21). The actual ion position was at the center of the twisted cube formed by eight keto oxygens of two stacked guanine tetrads. In order to demonstrate the role of the coordinated ion, 7-mer G-quadruplex was also constructed without any coordinated ion. These 7-mer quadruplex structures were surrounded by additional 24 Na^+ counter ions. The counter ions were placed 6Å from each of the phosphorus atoms, along the bisector of the two pendant oxygens, using the EDIT module of AMBER. In each system, DNA, coordinated ions and counter ions were then placed in a pre-equilibrated box of TIP3P water molecules. The periodic box of water was extended to a distance of 5Å from DNA and counter ions. In the subsequent analysis, Na^+ and K^+ ion

coordinated quadruplex systems are referred to as PA-Na and PA-K whereas the quadruplex without any initial coordinated ion is denoted as the PA structure. Average box dimension in the three simulations are around 32.9Å × 35.8Å × 35.8Å with the total number of water molecules included in the simulation varied from 1120 to 1102, depending on the solute molecule. Molecular dynamics was performed under NPT condition with SANDER module of AMBER 4.1 program (50) using the PARM 94 all atom force field and Particle Mesh Ewald method (PME) was used for the calculation of electrostatic interactions (51). The AMBER force field compatible Aqvist parameters (52) were used for the ions, viz: r_{eq} = 1.868Å, ε_{min} = 0.00277 kcal/mol for Na^+ and r_{eq} = 2.658Å, ε_{min} = 0.000328 kcal/mol for K^+ ion. The PME technique has been shown earlier to give stable trajectories in molecular dynamics simulation of solvated DNA duplex molecules (53-57). The net residual charge in the Na^+ or K^+ coordinated structure was neutralized using an option available in AMBER. The PME grid spacing was ~1.0Å. It was interpolated on a cubic B-spline, with the direct set tolerance set to 0.000001. Periodic boundary conditions were imposed in all directions. All solute-solute non-bonded interactions were calculated without any cut-off distance, while a non-bonded residue based cut-off distance of 9Å was used for the solvent-solvent and for the solute-solvent interactions. The non-bonded pair list was updated every 20 steps and the SHAKE algorithm was applied to constrain the covalent bonds. A time step of 2 fs was used and the structures were saved after every 100 steps, i.e. at every 0.2 ps interval, for the entire duration of the MD run.

Initial systems were energy minimized to an r.m.s gradient of 0.1 kcal/mol- Å. All the waters and surrounding counter ions were subjected to 20 ps dynamics at 100K, keeping DNA and coordinated ions fixed, followed by an energy minimization of the entire system. The quenched system was then heated slowly, from 0K to 300K, by coupling to a heat bath whose temperature was raised at the rate of 50K for every 2 ps of MD run. The system was equilibrated for another 88 ps and the production simulation was continued for a further 1 ns during which the structures were coupled to a heat bath at 300K with a coupling constant of 0.1 p_s^{-1}. MD average structures are obtained from the coordinates saved between 100 ps to 1100 ps and for the subsequent analysis, this average structure has been used without any further processing. All the structural parameters are calculated using the program NUPARM (58,59). All the trajectory plots are created using the MATLAB package.

Results and Discussion

Parallel Quadruplexes with Na^+ or K^+ Coordinated Ion Retain Similar Features

The root mean square (rms) deviation with respect to the initial energy minimized structure is calculated for all the parallel quadruplex structures. All simulations give stable rms trajectories as seen in Figure 2. The rms deviation of base atoms (shown in red lines) in all the three simulations are 0.8 to 1.0Å less than the corresponding backbone atoms (shown in green lines), indicating less movement of base atoms in comparison to backbone atoms. This is also observed in earlier DNA simulation (25,60). Average rms deviation (as shown on the right hand side of the Figure 2) with respect to initial MD structure is largest for the PA structure, as compared to Na^+ ion and K^+ ion coordinated structures, indicating that during the MD simulation, the quadruplex without any coordinated ion undergoes largest structural change. It is also observed that fluctuations of guanine base atoms with respect to their mean positions is smallest for the quadruplex with coordinated K^+ ion and largest for quadruplex without any coordinated ion, as indicated by the standard deviation values (in parentheses) on the right hand side of the Figure 2. This indicates that the G-tetrads with coordinated K^+ ion have less structural freedom than the Na^+ ion coordinated tetrads. In order to evaluate the differences between different MD average structures, the middle four nucleotides (3^{rd}, 4^{th}, 5^{th} and 6^{th} nucleotides) of PA-K and PA structure are super imposed on PA-Na structure and shown in Figure 3. It is noticed that the rms deviation between PA-Na and PA-K

structures is small (0.53Å), while deviation is larger between the PA-Na and PA structures (rms deviation is 1.15Å), indicating that the base and backbone geometry of PA is considerably different from PA-Na and PA-K structures. This is apparent from the snap shots of the three parallel quadruplex structures at the end of the simulation, which are shown in Figure 4A-C. A detailed analysis was carried out to pinpoint the cause of these variations.

Geometry and Interaction Energy Within a G-tetrad and Stacking Energy Between Successive G-tetrads

Base interaction energies within a G-tetrad in all the three structures were calculated during the simulation and the average interaction energies for each G-tetrad over 100 to 1100 ps simulation are shown in Table I. The base-base interaction energies are found to be directly related to the hydrogen bonding scheme and O6—O6 distances within the G-tetrad, which are listed in Table II for all three structures and discussed later in detail. Interaction energy within the G-tetrad in PA structure is more favourable than the other two structures. This is mainly due to the effect of very strong attractive energy calculated by the AMBER forcefield, for the electrostatic interaction between the coordinated Na^+ ion and O6 atoms in guanine bases. In the presence of a coordinated ion, guanine bases in the G-tetrad rotate about the helix axis and bring the keto oxygens closer together, leading to slightly unfavourable electrostatic energy for the bases alone, but this is more than compensated by the strong attractive ion-G-tetrad interaction energy. In the case of PA-Na structure, reorientation within the G-tetrad is more pronounced in the middle part of the 7-mer quadruplex. Therefore, interaction energies within the terminal G-tetrads in 7-mer PA-NA structure are more favourable than those in the middle as seen in Table I. Same trend is observed in the PA-K structure, where guanine bases in terminal G-tetrads have more favourable interaction energy. The 3rd and 5th tetrads undergo largest rotational motion of guanine bases in PA-K structure, giving rise to positive electrostatic component which makes the overall interaction energy between the bases unfavourable (Table I). However, if the interaction energy between the coordinated ion and guanine tetrads is included (on an average, this contribution is -124.0 kcal/mol for PA-Na and -116.4 kcal/mol for PA-K structure), then the total energy for each tetrad, alongwith one associated ion, is much more favourable in PA-Na and PA-K structures than in the PA structure.

Table I

Interaction energies[a] within the G-tetrad in PA-Na, PA-K and PA structures are shown along with average crystal structure (21) value. Total interaction energy is divided into van der Waals (vdW) and electrostatic (e.s.) component. Energies (in kcal/mol) are averaged over 100-1100 ps of dynamics. Standard deviations are given within parentheses, below each value.

	PA-Na			PA-K			PA		
	vdW	e.s.	Total	vdW	e.s.	Total	vdW	e.s.	Total
Tet-1	-4.2	-37.1	-41.3	-4.0	-50.3	-54.3	-3.3	-44.9	-48.2
	(2.2)	(9.0)	(7.8)	(2.3)	(6.7)	(6.0)	(1.8)	(9.4)	(8.8)
Tet-2	-4.3	-26.6	-30.9	-5.2	-29.2	-34.4	-1.4	-61.5	-62.9
	(2.9)	(12.4)	(11.0)	(2.1)	(7.5)	(7.0)	(1.8)	(4.2)	(3.4)
Tet-3	-5.4	-11.9	-17.3	-7.5	3.7	-3.8	-0.8	-63.8	-64.6
	(2.1)	(9.0)	(8.6)	(1.6)	(17.5)	(17.3)	(2.7)	(5.1)	(4.2)
Tet-4	-4.8	-9.4	-14.2	-6.5	-20.5	-27.0	-1.3	-62.3	-63.6
	(2.2)	(7.6)	(7.0)	(2.3)	(11.0)	(9.7)	(2.3)	(4.7)	(4.3)
Tet-5	-5.1	-12.3	-17.4	-7.6	8.3	0.7	-1.3	-61.5	-62.8
	(2.1)	(8.5)	(8.2)	(1.7)	(15.9)	(16.0)	(2.3)	(4.6)	(4.2)
Tet-6	-4.5	-20.7	-25.2	-5.2	-28.9	-34.1	-1.5	-58.4	-59.9
	(2.3)	(9.7)	(9.2)	(2.3)	(9.6)	(8.5)	(2.7)	(7.3)	(6.4)
Tet-7	-4.0	-35.9	-39.9	-4.1	-47.9	-52.0	-3.3	-46.7	-50.0
	(3.0)	(8.5)	(7.3)	(2.1)	(7.0)	(6.4)	(2.7)	(12.6)	(11.6)
Crystal	3.3	-57.0	-53.7						
Structure	(1.5)	(1.5)	(1.5)						

[a]AMBER 4.1 does not have separate 10-12 function for representing hydrogen bonds, instead the interaction is included as a 6-12 function with revised charges and van der Waals parameters for the relevant atoms.

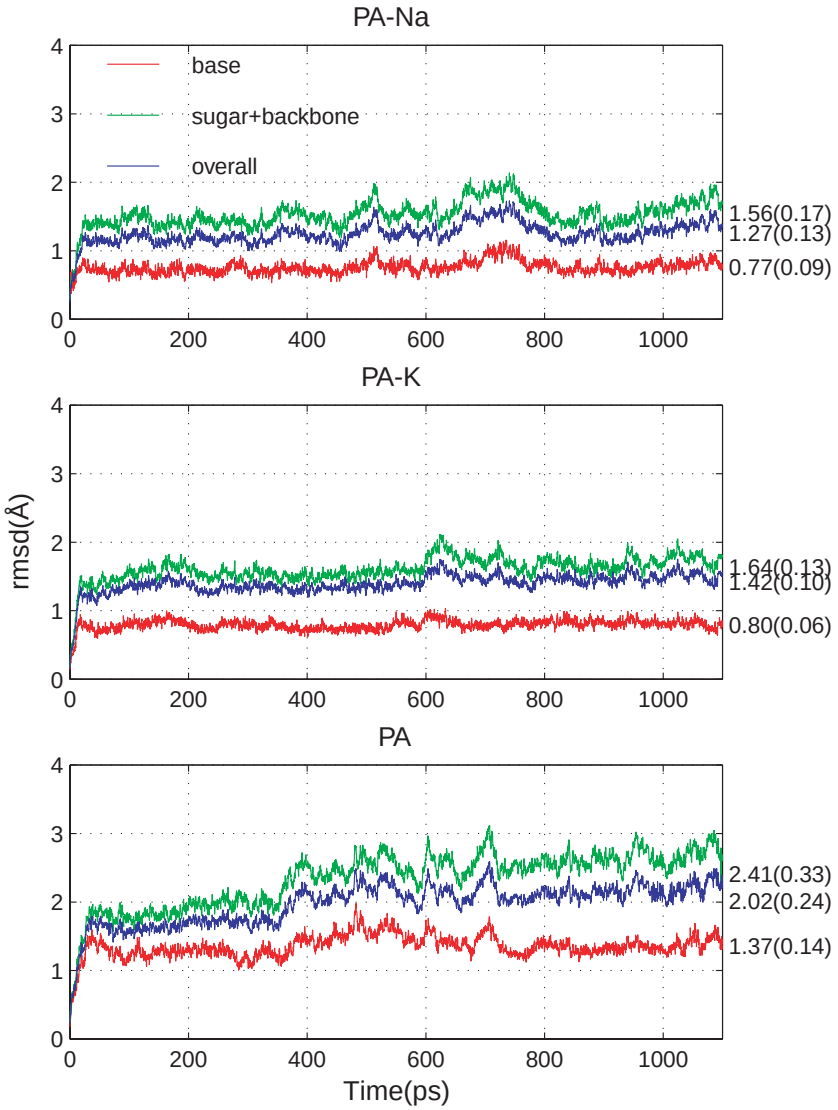

Figure 2: Root mean square (rms) deviation profiles, during the MD simulation, of three d(G_7) parallel quadruplexes, with respect to their respective initial energy minimized structures. The mean value of rmsd between 100 to 1100 ps interval is indicated on the right hand side of each plot. The standard deviation is given within parenthesis.

In order to understand the effect of coordinated ions on the stacking of G-tetrads, stacking energy between the successive G-tetrads was also monitored for all the structures over 100 to 1100 ps of dynamics. If we consider only guanine base stacking, PA structure has most favourable stacking energy. The van der Waals component of all three structures vary between -40 to -45 kcal/mol (data not shown) whereas the electrostatic component of base stacking energy in PA structure contributes about +10 kcal/mol, while it is much larger in the ion coordinated structures. In the absence of any coordinated ion, O6 atoms in G-tetrad stay apart to minimize O6-O6 repulsion, leading to less repulsive electrostatic component. Thus, overall base stacking energy (~ -33.0 kcal/mol) in PA structure is more favourable than in PA-Na and PA-K structures (~ -2.0 and ~ -5.0 kcal/mol respectively). However, as in the case of G-tetrad energy, inclusion of the energy contribution due to coordinated ions in stacking energy calculation makes the coordinated ion structures more favourable than the PA structure, as shown in Table III, which lists the average stacking energies between 3rd and 4th, 4th and 5th and between 5th and 6th G-tetrads in PA-Na, PA-K and PA structures, during 100-1100 ps of molecular dynamics simulation. The G-tetrad and the coordinated ion on its 5′ side are considering as one group, for ion coordinated quadruplexes. Thus, total stacking energy in this case consists of the guanine tetrad stacking energy, the interaction energy between coordinated ions, as well as interaction energies between the coordinated ion with its neighbouring G-tetrad on the 3′ side, while in the case of PA structure, interaction energies between successive G-tetrads constitute the total stacking energy.

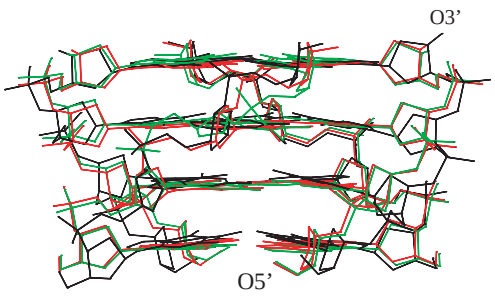

Figure 3: Middle four nucleotides (3rd, 4th, 5th and 6th) in MD average PA-K (green lines) and PA structures (black lines) are superimposed on the Na^+ ion coordinated PA-Na structure (red lines). The rms deviations between the PA-K (green) and PA (black) structures with respect to the PA-Na structure (red) are 0.53 and 1.15Å respectively

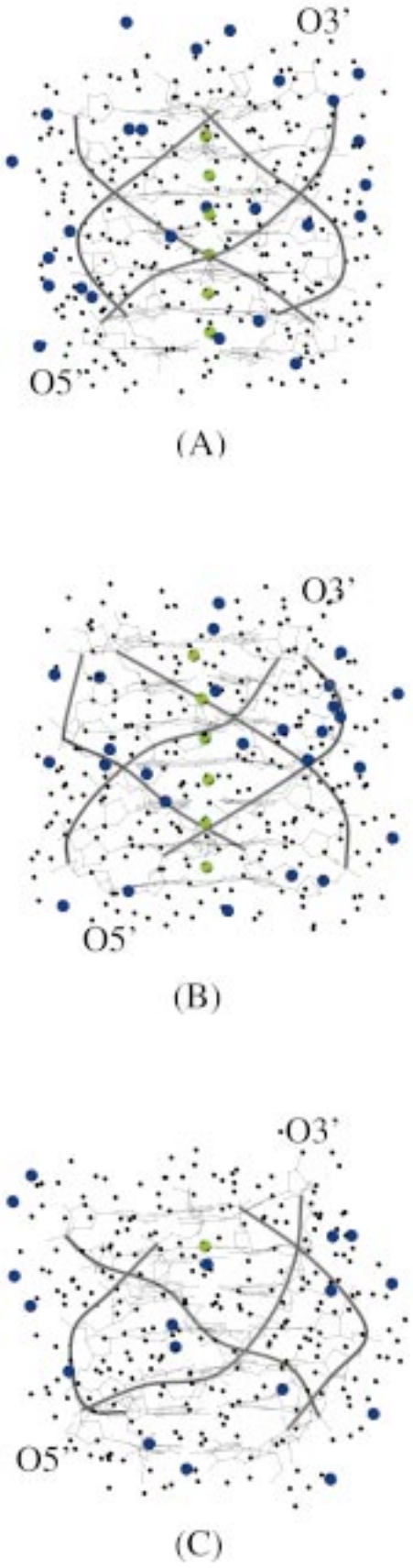

It is observed form Table III that stacking energy for the PA-Na structure is much more favorable than for the Na^+ ion coordinated crystal structure (21), even though the van der Waals component of stacking energy is more favourable for the latter. It may be mentioned that a few cycles of energy minimization makes the two structures comparable. The stacking energy between 4th and 5th G-tetrad in PA-K structure is found to be marginally less favourable than the stacking energy between 3rd and 4th or between 5th and 6th tetrads. This is due to more favourable electrostatic energy between the coordinated ion and the 3rd and 5th G-tetrads, as compared to the 4th and 6th tetrads due to differences in the tetrad geometry, as discussed above and shown in Table IIB. The van der Waals component is marginally more favourable in PA-Na structure than in PA-K structure, making the total stacking energy for PA-Na slightly more favourable. This indicates that the Na^+ ion is more readily accommodated in the quadruplex cavity.

Behaviour of Coordinated and Solvent Counter Ions

The behaviour of cations, inside the quadruplex cavity is different from that in the surrounding solvent medium and the behaviour of the coordinated Na^+ ions is also different from that of the coordinated K^+ ions. It is observed that in case of PA-Na structure, coordinated Na^+ ions at both terminii can move out from the central cavity of the quadruplex, as indicated by the related Na^+—O6 distance trajectories, shown in Figure 5. The Na^+ ion, coordinated between the two successive G-tetrads at the 5′- terminus of the parallel quadruplex transiently moves out of the DNA core between 100 to 205 ps and 755 to 855 ps of dynamics as observed from the elongated distance between first Na^+ ion and O6 atoms of second tetrad whereas the distances between first Na^+ ion and O6 atoms of first tetrad remain in the ~2.5Å range. Similar type of axial movements of coordinated Na^+ ion is transiently observed at the 3′- terminus of the PA-Na structure. However, all the Na^+—O6 distances are invariably smaller than those observed in the crystal structure (mean value 2.91Å). The larger movement of two terminal Na^+ ions is also reflected in the slightly lower average values and greater fluctuation in their interaction energy with the DNA, as compared to the middle four ions (trajectories shown in Figure 6). The axial movement of K^+ ion, through the quadruplex cavity was not observed within our molecular dynamics time scale. No noticeable fluctuation is observed in related K^+—O6 distances as well as coordinated ion-DNA interactions, as seen in Figures 5 and 6 respectively. It is also observed that the root mean square deviations of the coordinated K^+ ions with respect to initial MD structure are significantly smaller than that of the coordinated Na^+ ions, indicating that during the simulations, deviations as well as fluctuations of coordinated Na^+ ions, from their initial positions, are larger than that of K^+ ions (data not shown). This is probably due to the larger radius of K^+ ion, which does not allow even transient in-plane coordination with G-tetrad and hence restricts free movement of K^+ ion along the central cavity.

During the MD simulation, solvated Na^+ counter ions in all the three parallel structures traverse quite large distances and can bind the phosphate groups as well as in the grooves. It is clearly observed that in all the structures, a few counter ions and water molecules are bound within the quadruplex grooves. During the molecular dynamics simulation, on an average, 5 Na^+ counter ions are within 3Å of PA-Na quadruplex structure whereas in case of PA-K and PA structures 6 counter ions are within 3Å of DNA. One counter ion in PA-Na structure is firmly (more than 65% of total dynamics time) bound to the phosphate group at 5′ end of second strand whereas two other counter ions occupy (for more than 50% of dynamics time) quadruplex grooves between 2nd -3rd and 3rd-4th strands. Four Na^+ counter ions in the PA-K structure are also within the grooves. These counter ions are mainly

Figure 4: Snap shots of the various parallel quadruplex structures at the end of the 1.1 ns simulations. The solvent counter ions (within 5.0Å cut off distance from quadruplex) are shown in blue (filled circles) and water molecules (within 3.0Å) as black dots. **(A)** PA-Na quadruplex with coordinated Na^+ ions. **(B)** PA-K quadruplex with coordinated K^+ ions. **(C)** The PA structure without any coordinated ion in the initial structure. Phosphodiester backbone is shown as a ribbon and filled green circles represent the coordinated cations. It is seen that one of the solvent ions in PA is now coordinated between tetrads 6 and 7.

bound to the pendant oxygen atoms of phosphate groups. Representative ion-DNA interaction energies for these groove bound solvent ions are shown in the last row of Figure 6. The mean interaction energy of these ions with DNA is about 100 kcal/mol more favourable than for the unbound ions, which however have better interaction with the surrounding water molecules.

In the case of PA structure, between 500-600 ps of dynamics simulation, one Na^+ ion moves from the solvent to the vacant coordination site within the DNA quadruplex (enters into the quadruplex cavity through the O3′ end). It is also observed that as soon as the ion enters the quadruplex cavity, it moves with slower speed along the central channel of the quadruplex and approaches the next tetrad. Its interaction

Table II

Average values of inter atomic distances (in Å) between potential hydrogen bond forming groups within the G-tetrad in the crystal structure (21), fibre model (18) and the MD average (A) PA-Na (B) PA-K (C) PA structures. In case of PA structure, the MD average structure was obtained from the coordinates saved between 600 to 1100 ps of dynamics. The distances between O6 atoms on adjacent and diagonal guanines in the tetrad, as well as between opposite corners of the twisted cube formed by O6 atoms on two neighbouring G-tetrads are also listed. Standard deviations are shown in parentheses. Average distances over all seven G-tetrads are shown in the last row of each table.

(A) PA-NA structure.

	N1--O6/H1--O6		N2--N7/H2--N7		N1--N7/H1--N7		O6-O6[a]	O6-O6[b]	O6-O6[c]
Crystal	2.87	1.94	2.83	1.85	3.78	3.05	3.18	4.50	5.44
Structure	(0.02)	(0.03)	(0.04)	(0.04)	(0.08)	(0.09)	(0.05)	(0.11)	(0.25)
Fibre	2.87	2.02	2.67	1.67	3.41	2.62	2.84	4.02	4.89
Model	-	-	-	-	-	-	-	-	-
Tet-1	2.93	2.03	2.81	1.85	3.51	2.79	3.00	4.24	4.99
Tet-2	3.06	2.24	2.86	1.92	3.25	2.46	2.81	3.97	4.89
Tet-3	3.23	2.47	2.94	2.04	3.09	2.23	2.71	3.83	4.89
Tet-4	3.27	2.53	2.96	2.07	3.05	2.18	2.70	3.81	4.91
Tet-5	3.24	2.49	2.95	2.04	3.08	2.23	2.71	3.84	4.92
Tet-6	3.12	2.32	2.88	1.95	3.19	2.38	2.77	3.91	5.05
Tet-7	2.95	2.07	2.84	1.88	3.47	2.74	2.97	4.20	
Mean	3.11	2.31	2.89	1.96	3.23	2.43	2.81	3.97	4.95
Std. dev.	(0.13)	(0.19)	(0.06)	(0.08)	(0.18)	(0.23)	(0.12)	(0.17)	(0.10)

(B) PA-K structure.

	N1--O6/H1--O6		N2--N7/H2--N7		N1--N7/H1--N7		O6-O6[a]	O6-O6[b]	O6-O6[c]
Tet-1	2.92	1.95	2.95	1.98	3.96	3.29	3.35	4.74	5.21
Tet-2	3.10	2.24	2.94	1.97	3.44	2.65	2.95	4.18	5.12
Tet-3	3.83	3.14	3.43	2.63	3.09	2.13	2.91	4.11	5.36
Tet-4	3.22	2.39	3.00	2.05	3.36	2.52	2.92	4.13	5.17
Tet-5	3.92	3.24	3.50	2.73	3.06	2.10	2.93	4.14	5.39
Tet-6	3.13	2.28	2.94	1.98	3.41	2.61	2.95	4.17	5.40
Tet-7	2.93	1.98	2.94	1.97	3.87	3.18	3.27	4.62	
Mean	3.23	2.46	3.10	2.19	3.46	2.64	3.04	4.30	5.27
Std. dev.	(0.38)	(0.49)	(0.24)	(0.32)	(0.32)	(0.43)	(0.17)	(0.25)	(0.11)

(C) PA structure**.**

	N1--O6/H1--O6		N2--N7/H2--N7		N2--O6/H2--O6		O6-O6[a]	O6-O6[b]	O6-O6[c]
Tet-1	3.29	2.53	3.82	3.21	3.05	2.31	4.56	6.40	7.40
Tet-2	3.13	2.27	3.52	2.79	3.09	2.24	4.37	6.17	6.65
Tet-3	2.88	1.94	3.16	2.35	3.22	2.40	3.94	5.57	6.56
Tet-4	3.02	2.15	3.40	2.68	3.06	2.19	4.23	5.99	6.94
Tet-5	3.18	2.35	3.61	2.95	2.90	1.97	4.57	6.45	6.50
Tet-6	2.95	1.99	3.16	2.28	3.51	2.75	3.78	5.33	5.45
Tet-7	2.97	2.05	2.89	1.93	4.19	3.58	3.13	4.43	
Mean	3.06	2.18	3.38	2.60	3.29	2.49	4.08	5.76	6.58
Std. dev.	(0.31)	(0.44)	(0.50)	(0.63)	(0.49)	(0.58)	(0.70)	(0.68)	(0.79)

[a]Distance between adjacent O6 atoms within a G-tetrad.

[b]Distance between diagonally opposite O6 atoms within a G-tetrad.

[c]Distance between O6 atoms at opposite corners of the twisted cube.

Table III

Stacking energy values in PA-Na, PA-K and PA structures are listed along with the crystal structure values. Stacking energies are averaged over 100-1100 ps of molecular dynamics simulation. In the case of 4-mer crystal structure (21), 2nd and 3rd tetrads are considered for stacking energy calculation whereas stacking energy between 3rd - 4th, 4th - 5th, and 5th - 6th tetrads are shown for PA-Na, PA-K and PA structures. Total stacking energy is divided into van der Waals (vdW) and electrostatic (e.s.) components and includes contribution from coordinated ions in case of the crystal structure, PA-Na and PA-K structures. All energy values are in kcal/mol. Standard deviation values are shown in parentheses.

	PA-Na			PA-K			PA		
	vdW	e.s.	Total	vdW	e.s.	Total	vdW	e.s.	Total
Tet34	-40.0	-23.5	-63.5	-34.4	-20.6	-55.0	-43.4	10.3	-33.1
	(2.0)	(6.3)	(5.6)	(2.6)	(8.3)	(8.3)	(1.3)	(2.1)	(1.9)
Tet45	-40.8	-20.8	-61.6	-35.3	-11.7	-47.0	-43.6	9.7	-33.9
	(2.0)	(5.0)	(4.3)	(2.2)	(6.1)	(6.4)	(1.4)	(2.7)	(2.2)
Tet56	-41.2	-16.5	-57.7	-34.9	-24.3	-59.2	-42.5	9.9	-32.6
	(1.7)	(5.6)	(5.3)	(2.4)	(7.7)	(7.9)	(1.5)	(2.8)	(2.3)
Crystal Structure	-46.1	12.3	-33.8						

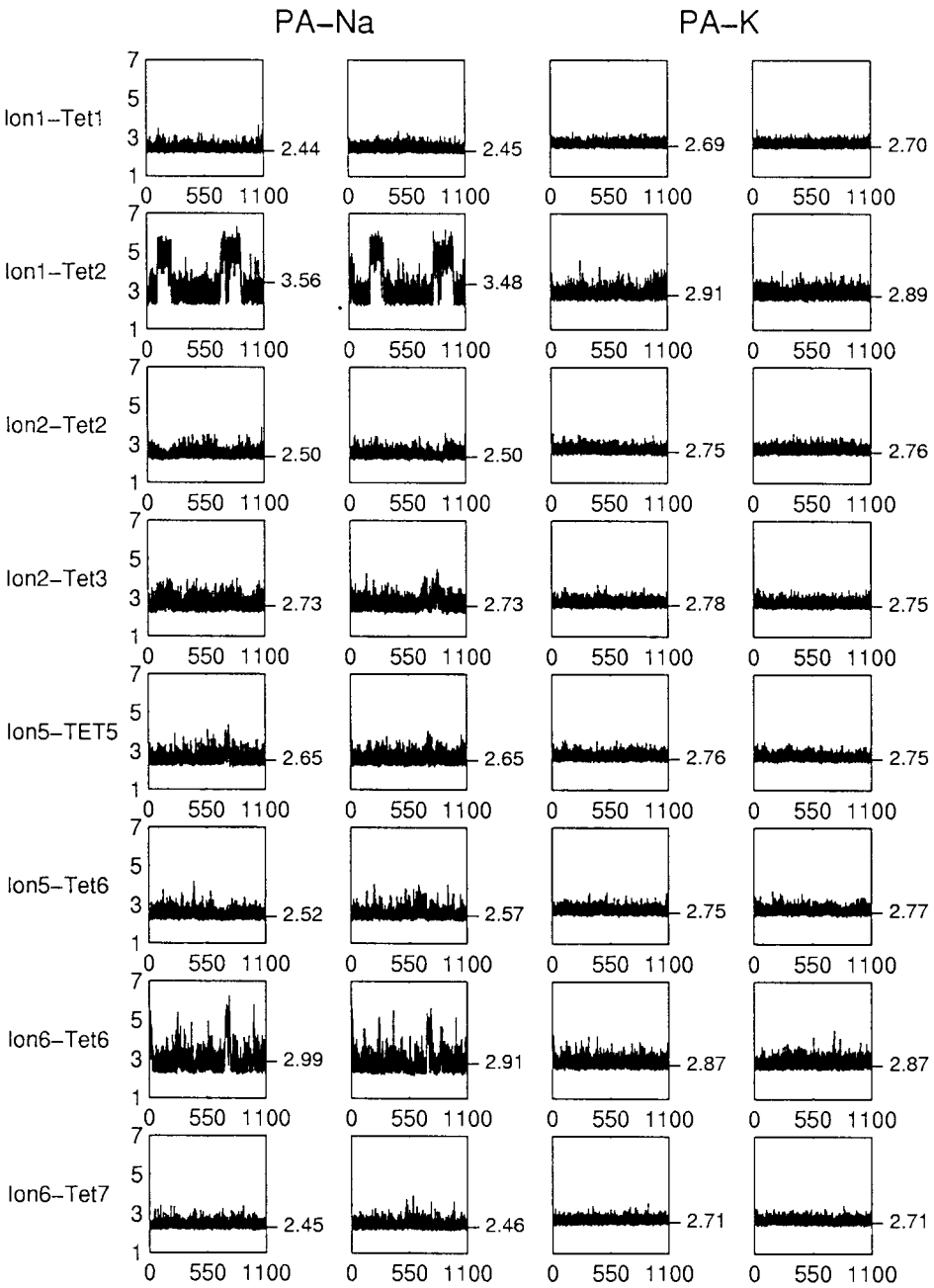

Figure 5: Trajectories showing the distances between the coordinated ions and neighbouring O6 atoms in the PA-Na and PA-K structures are shown. Only two of the coordinated ions, at the 5′ and 3′ ends of the quadruplex and their distances from O6 atoms in the first and second strands are shown. The two middle ions are relatively immobile and hence data corresponding to them is not shown. Average distances over 100-1100 ps of dynamics are written at the right hand side of each plot. Time (in ps) is along x-axis and ion—O6 distances in Å are along y-axis.

energy with DNA improves dramatically, as seen in Figure 6 for the PA structure (first row of last column). At the end of the 1.1 ns dynamics, one more solvent counter ion is seen to approach towards the quadruplex cavity through the O5′ end (as seen in Figure 4C). Three of the solvent counter ions in the PA structure bind well inside the grooves and stay close to the guanine base atoms, particularly N7 and N3 atoms and their interaction energy trajectories are also shown in Figure 6, along with that for one representative unbound ion. All groove bound counter ions in the three quadruplex structures can move within their respective groove, though their movements are slower than that of bulk counter ions.

Hydration Patterns in the Quadruplex Grooves

The hydration pattern within the four quadruplex grooves, in the three structures are clearly observed during the molecular dynamics simulation. Since all the four strands in these quadruplexes are parallel, the quadruplexes have four symmetrical grooves. Interestingly, the hydration patterns are also equivalent in four quadruplex grooves. A string of hydrogen bonded water molecules are observed within the grooves, in all the three structures. In the case of PA-Na and PA-K structures, the 2-amino group and N3 atom on the exposed face of the guanine bases are the most favorable binding sites for groove binding water molecules. The water molecules are localized (within 3Å radius) near N2 and N3 atoms of guanine bases and form hydrogen bonds. Snap shot of the first two strands in the PA-Na structure and groove binding water mole-

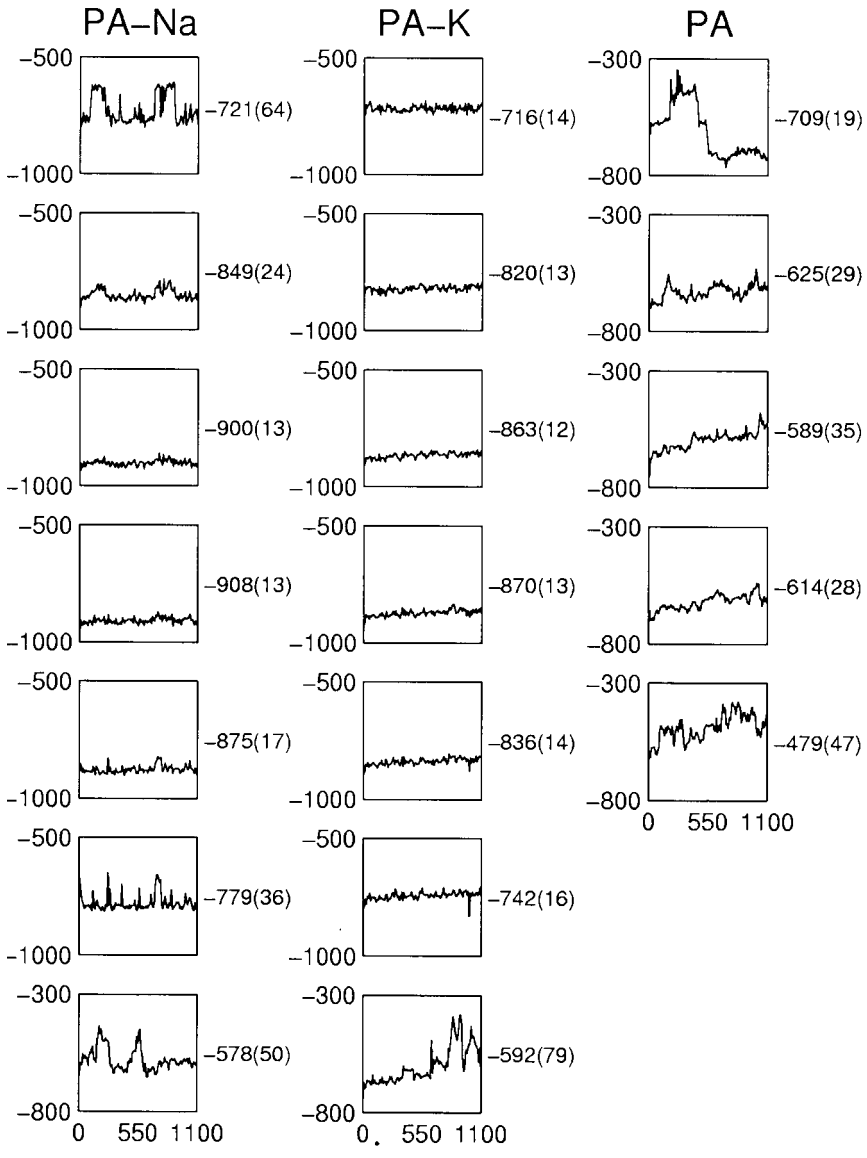

Figure 6: Trajectories showing the individual ion-DNA interaction energy during the MD simulations. Time (in ps) is along x-axis and interaction energy (in kcal/mol) is along the y-axis. Average interaction energy values alongwith their standard deviations in the period between 100 to 1100 ps, are indicated at the right hand side of each plot. In the case of PA-Na and PA-K panels, the first six rows represent interaction energy of coordinated Na^+ or K^+ ions with DNA, with the coordinated ion at the 5′end being at the top, while the last row shows interaction energy of DNA with a representative groove bound Na^+ counter ion in each of the structures. In the case of PA, the first row shows the interaction energy of DNA with the Na^+ counter ion which moves inside the quadruplex channel after 600 ps of dynamics, with the average value corresponding to the range between 600-1100 ps. Next three rows represent interaction energies of groove bound Na^+ counter ions with DNA whereas, last row shows the interaction energy for a representative unbound counter ion.

cules, at the end of the 1.1 ns simulation is shown in Figure 7. However, water molecules have a preference for N2 atom over N3 atom. Due to in-plane rotation of guanine bases, the 2-amino groups moved out, into the grooves and are thus more exposed to the solvent water molecules. On the other hand, N3 atoms are partially blocked from hydration due to nearby sugar moiety. The guanine hydration patterns in PA-NA and PA-K structures have some similarities to that of quadruplex crystal structure (21) and Z-DNA whereas, in A and B-DNA crystal structures, N2 position remains almost unhydrated (61). In the absence of coordinated ions, a few water molecules enter the quadruplex cavity through the ends of quadruplex and occupy the same position between the G-tetrads where the coordinated ions are present in the other two structures. The N7 atoms in the PA structure are comparatively more exposed to solvent water molecules when compared to PA-Na and PA-K structure due to the different base orientation within the G-tetrad as discussed in the next section. Specifically, N7 atoms of 4^{th} and 5^{th} guanine bases, in the first strand are two good water binding sites. However, 2-amino groups and N3 atoms in PA structure remain the most favourable binding sites for water molecules.

Effect of Coordinated Ions on Hydrogen Bonding Patterns Within G-tetrads

The G-tetrad in the starting fibre model as well as crystal structure of parallel quadruplex with coordinated Na^+ ions contain cyclic N1-H1··O6 and N2-H2···N7 hydrogen bonds (Hoogsteen type) between adjacent guanines, leading to eight hydrogen bonds per G-tetrad (as shown in Figure 1). Inter atomic distances between potential hydrogen bonding groups and distances between different O6 atoms in the MD average PA-Na and PA-K structures are tabulated in Table II (A-B). Hydrogen bonding patterns of terminal G-tetrads in PA-Na and PA-K structures are quite similar to crystal structure as seen by comparing Figures 8A and 8C with Figure 1 and also from Tables IIA and IIB. In the case of inner G-tetrads in PA-Na, due to the strong attractive interaction between coordinated ions and O6 atoms, G-bases within a tetrad undergo a rotational motion, which makes original N1···O6 Hoogsteen type hydrogen bonds about 0.3-0.4Å longer than the fibre model values (starting structure). Simultaneously N1 and N7 atoms come within hydrogen bonding range (shown in Figure 8B). Similar type of bifurcated or three centered hydrogen bonds within Na^+ ion coordinated G-tetrads are observed in recent MD studies on the 4-mer crystal structure (27). In case of PA-K, the 4^{th} G-tetrad shows a bifurcated hydrogen bonding scheme similar to that in the PA-Na structure, whereas the larger rotational motion of guanine bases in the flanking tetrads, leads to a G-tetrads stabilized only by cyclic N1-H1···N7 hydrogen bond as shown in Figure 8D. However, the two terminal tetrads at both ends of PA-K structure retain standard Hoogsteen hydrogen bonding scheme with slightly elongated N1-H1···O6 hydrogen bonds.

In the case of PA structure, potential hydrogen bond distances as well as distances between various O6 atoms, as listed in Table IIC, were calculated from the MD average structure obtained from the coordinates saved between 600 to 1100 ps of dynamics, after the entry of a Na^+ ion into the central cavity. In the absence of coordinated ions, (as in the case for tetrads 1 to 5) the base rotation within the inner G-tetrad in PA structure is in opposite direction to that found in quadruplexes with coordinated Na^+ and K^+ ions and the O6 atoms are almost equidistant from N1 and N2 atoms of the adjacent guanine. Thus, during the molecular dynamics simulation, while a few N2-H2···N7 hydrogen bonds are broken, N2 and O6 atoms come within hydrogen bond distance. In fact, N2-H2···O6 hydrogen bond distances are shorter than N2-H2···N7 hydrogen bond distances (see Table IIC). However, there are large fluctuations in hydrogen bond distances in the PA structure. Recent ab initio study (26) on Hoogsteen-bonded G-tetrad also predict this type of bifurcated hydrogen bond arrangement, on the other hand, MD simulation of the 4-mer parallel quadruplex structure without any coordinated ion (27) reported a distorted structure, in which one strand has slipped with respect to the other three strands in the quadruplex. As mentioned above, after 550 ps of dynamics run, we find that one

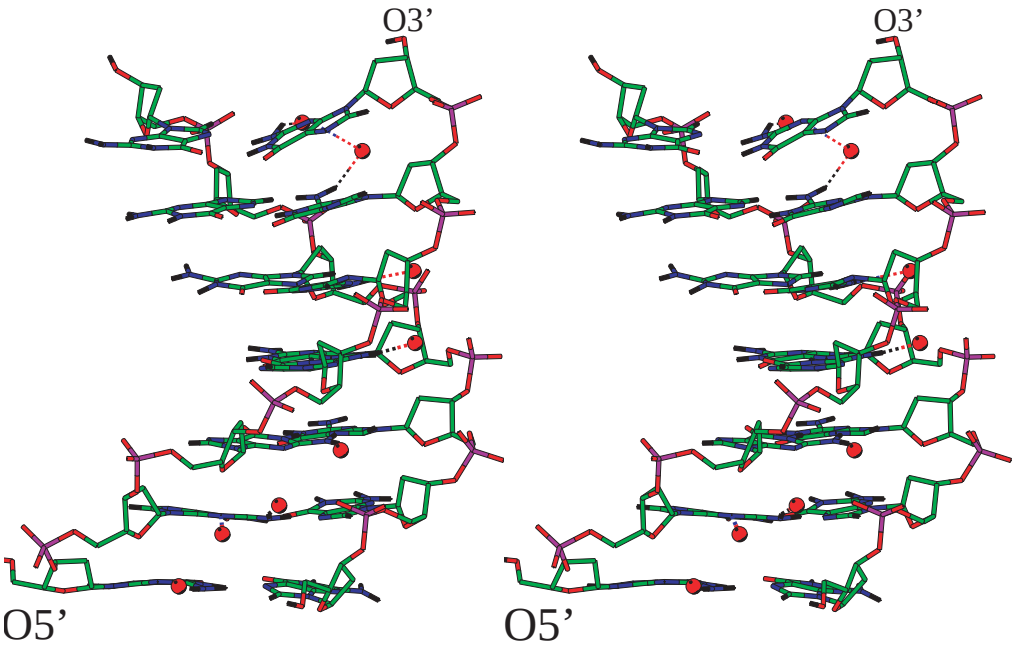

Figure 7: A stereodiagram showing the 1st and 2nd strands of the PA-Na quadruplex structure alongwith the groove bound water molecules, at the end of 1.1 ns dynamics. Oxygen atoms of water molecules, which are within 3Å of guanine bases and within the quadruplex groove, formed by the two strands are shown as red circles. Dotted lines connect the base atom and oxygen atom of a water molecule.

solvent Na^+ ion enters the DNA cavity through the 3′ terminal and occupies the empty cavity between the 6th and 7th tetrads. It is clearly observed that the geometry of the tetrads at the 3′ terminus, before and after 550 ps are different from each other. The hydrogen bonding scheme of 5th and 7th tetrads obtained from the two average structures (coordinates saved between 100 to 600 ps and 600 to 1100 ps respectively) are shown in Figure 9A-D. During the first 600 ps dynamics, both

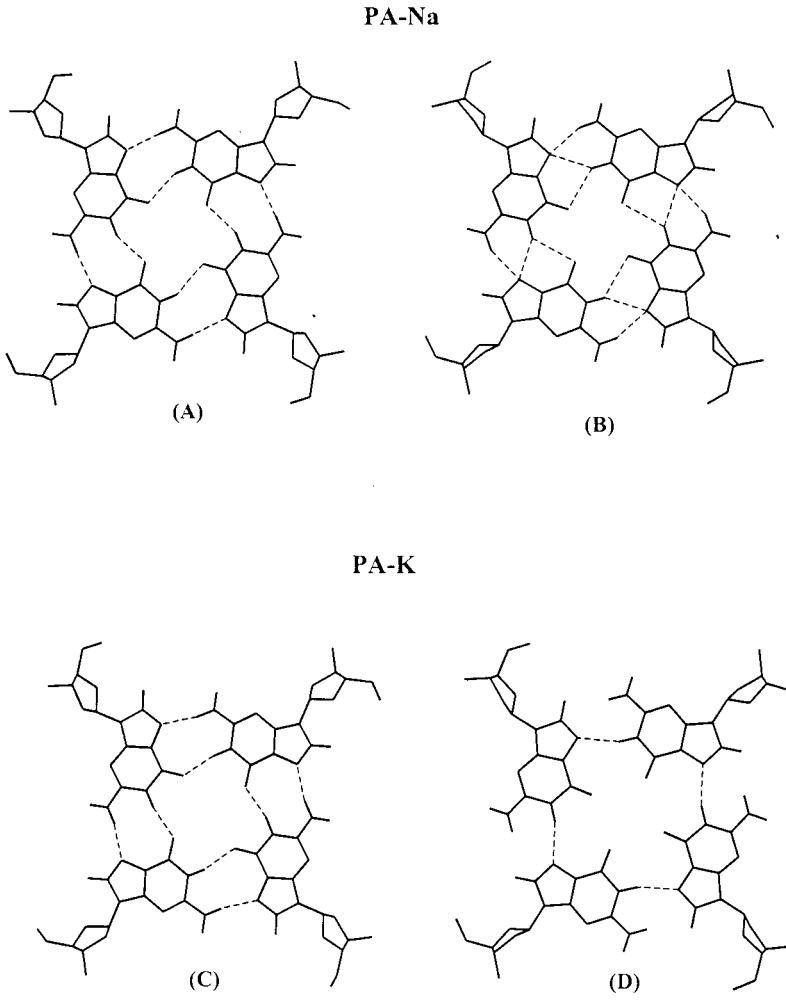

Figure 8: Hydrogen bond patterns in the 1st and 3rd tetrads in MD average PA-Na and PA-K structures. **(A)** and **(C)** represent the 1st tetrad at the 5′ end in PA-Na and PA-K structures respectively whereas **(B)** and **(D)** show the 3rd G-tetrad in these structures. Dotted lines indicate hydrogen bonds with hydrogen to acceptor distances < 2.6Å. The effect of coordinated ion is clearly seen in the altered hydrogen bond patterns of the 3rd tetrad in both structures.

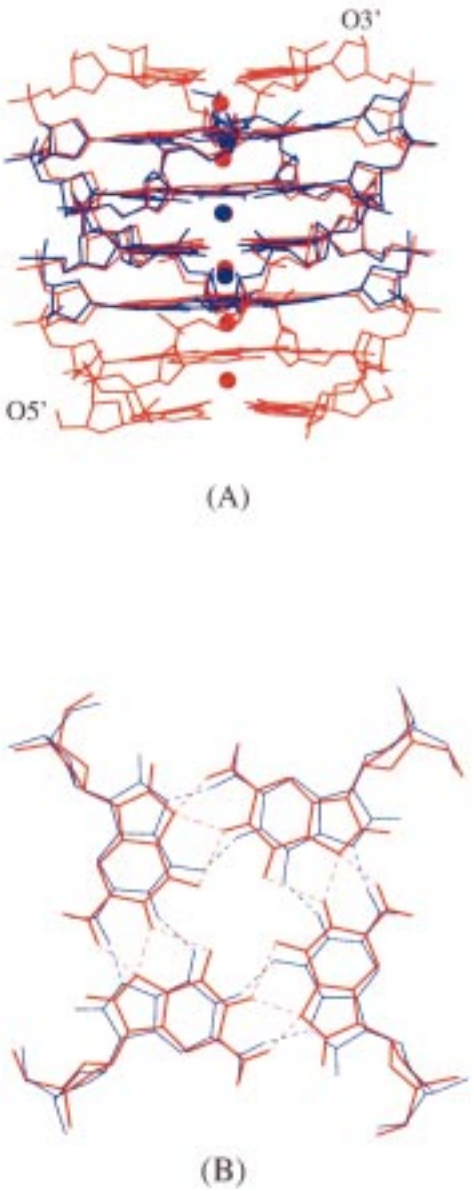

Figure 10: **(A)** The G4 stretch of the d(TG_4T) quadruplex crystal structure (in blue lines) (21) is shown superimposed on the 3rd, 4th, 5th and 6th guanine nucleotides of the 7-mer MD average PA-Na structure (in red lines). The 5′ and 3′ ends of strand 1 are indicated by O5′ and O3′. Coordinated Na^+ ions in the crystal (in blue filled circles) and MD average structure (in red filled circles) are also shown. The rms deviation for all atoms in the equivalent fragment of PA-Na with respect to the crystal structure is 0.71Å, while it is 0.54Å for the guanine tetrads alone. **(B)** Second G-tetrad of the d(TG_4T) quadruplex crystal structure (in blue lines) is shown superimposed on middle G-tetrad of MD average PA-Na structure (red lines). Dotted lines indicate the hydrogen bonds in both the G-tetrads, for which hydrogen to acceptor atom distance is < 2.6Å.

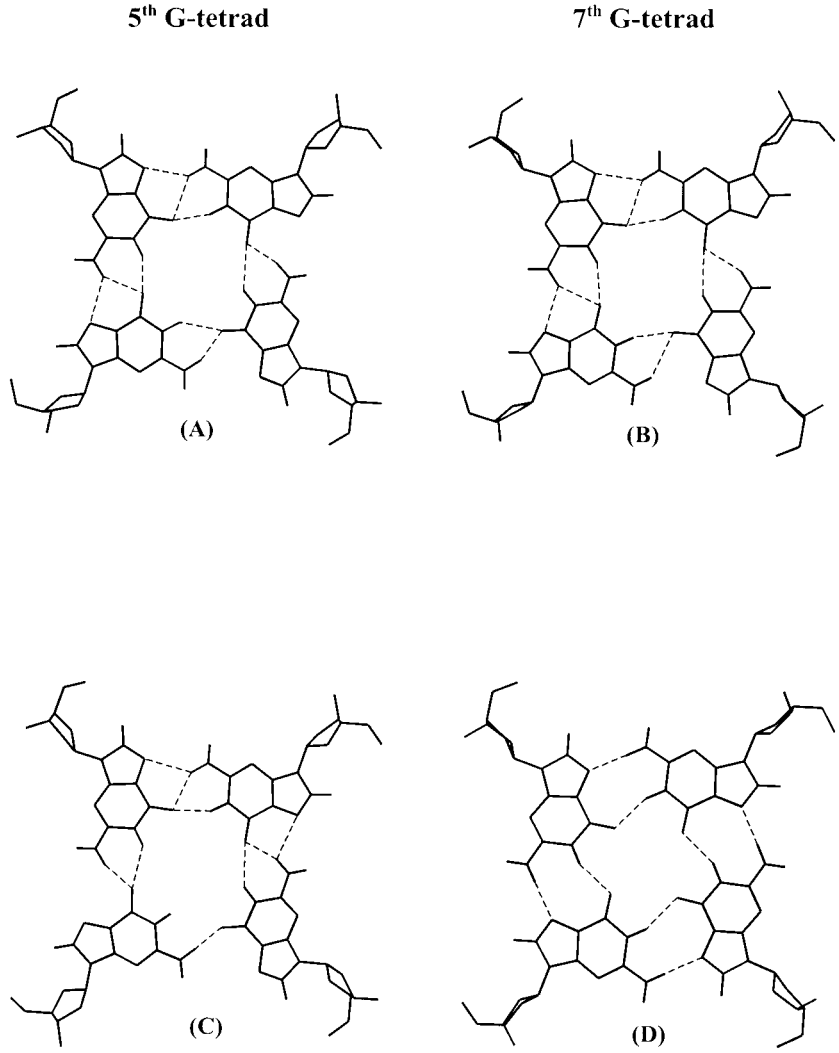

Figure 9: Hydrogen bonding scheme in two representative G-tetrads during the MD simulation of PA structure. **(A)** and **(B)** represent the 5th and 7th (3′ terminus) tetrads respectively, in the average structure obtained from the coordinates saved between 100-600 ps. **(C)** and **(D)** represent the same tetrads in the average structure from the coordinates saved between 600-1100 ps of dynamics, after the entry of the Na^+ ion into the central cavity. Dotted lines indicate the hydrogen bonds for which hydrogen to acceptor atom distances are ≤ 2.6.

these tetrads at 3′ end show bifurcated hydrogen bonds similar to those in the middle tetrads of PA structure (as seen in Figure 9A and 9B). As soon as the Na^+ ion enters the quadruplex cavity, the strong attractive interaction between the ion and O6 atoms rotates the guanine bases, leading to normal Hoogsteen hydrogen bonds. Thus, after 600 ps of dynamics, the 6th and 7th G-tetrads in PA structure show standard Hoogsteen type hydrogen bond (Figure 9D), while the 5th tetrad shows a bifurcated hydrogen bond pattern (shown in Figure 9C), which is similar to that seen for the other tetrads in the PA structure.

Thus, it is observed that coordinated K^+ ion distorts the G-tetrads more than the Na^+ ion, whereas quadruplexes without any coordinated ion exhibit a different type of hydrogen bonding scheme, which is also a variant of the standard Hoogsteen type hydrogen bonds. During the MD simulation, a wide spectrum of hydrogen bonding patterns are observed due to the rotational motion of guanine bases within the various G-tetrads and coordinated cation plays a crucial role.

Guanine base rotation about the quadruplex axis is also indicated by the O6—O6 distances between adjacent, as well as diagonal guanine bases within a G-tetrad (listed in Table IIA-C). Adjacent and diagonal O6—O6 distances in middle tetrads

are considerably smaller than in the terminal tetrads, in both PA-Na and PA-K structures, as well as in the crystal structure. Due to the presence of larger K^+ ion, these O6—O6 distances in PA-K structure are longer than in the PA-Na structure. Since the guanine base rotation within the G-tetrad in PA structure is in opposite direction to that found in PA-Na and PA-K structure, O6 atoms within a G-tetrad move further apart. Consequently, adjacent and diagonal O6—O6 distances within a G-tetrad as well as between neighbouring G-tetrads become longer than those found in PA-Na and PA-K structure.

Backbone Torsion Angles and Structural Parameters in Different G-quadruplexes

The backbone torsion angles, glycosidic torsion angles (χ) and pseudorotation phase angles (P) of PA-Na, PA-K and PA structures have been calculated during the simulations and average values for each strand are listed in Table IV. During the molecular dynamics of PA-Na structure, O5′ terminal γ angle in second strand undergoes a transition to *trans* region. All other backbone torsion angles in PA-Na structure are well behaved and fluctuate within canonical B-DNA range i.e. α, β, γ, ε and ζ torsion angels are in *gauche*$^-$ (g^-), *trans (t), gauche*$^+$ (g^+), *trans (t)* and *gauche*$^-$ (g^-) region respectively. Some of the torsion angles in both the PA-K and PA structures show large fluctuation and undergo transition to non-canonical regions. A few of the α, β and γ torsion angles in one strand of PA-K structure undergo transition from their respective canonical region to *t*, g^+ and *t* region. It is also observed that, the 5′ terminal tetrad in PA structure distorts during the simulation. Consequently, 5′ terminal ε and ζ angles in 2nd, 3rd and 4th strand undergo a transition to g^- and g^+ region respectively. It is also seen that the ε torsion angle of the fourth nucleotide in the third strand of PA structure undergoes a transition from *t* to g^- region and a correlated transition in ζ from g^- to *t* is also observed. In comparison with PA-Na and PA-K structures, larger fluctuations in backbone torsion angles are observed in PA structure (as seen from the standard deviation values listed in Table IV). The glycosidic torsion angles for all the three parallel quadruplexes remain in *anti* orientation while the pseudorotation phase angles (P) oscillate between O4′-*endo* and C1′-*exo* region, as reported in other DNA simulations with AMBER forcefield (56,57). However, a few of the sugars in the PA structure show puckering between C3′-*endo* and C4′-*exo* region.

Table IV

Mean values of the six backbone torsion angles (α-ζ), the glycosidic torsion angle (χ) and the pseudorotation phase angle (P) are listed during 100-1100 ps of dynamics. In the case of PA-Na, PA-K and PA structures, angles are averaged over the full 7-mer strand of the quadruplex. Average torsion angles in the crystal structure (21) are also shown. All angles are in degrees and standard deviations are shown in parentheses.

	PA-Na				PA-K				PA				Crystal Structur
	Strand 1	Strand 2	Strand 3	Strand 4	Strand 1	Strand 2	Strand 3	Strand 4	Strand 1	Strand 2	Strand 3	Strand 4	
α	292	292	291	292	293	293	293	269[c]	290	284	283	288	290
	(11)	(11)	(11)	(11)	(11)	(11)	(11)	(51)	(11)	(24)	(22)	(14)	(6)
β	174	173	173	173	173	173	174	159[d]	174	172	169	163	189
	(10)	(11)	(10)	(11)	(11)	(11)	(11)	(41)	(12)	(11)	(14)	(24)	(12)
γ	57	75[a]	57	57	73[b]	54	57	91[e]	57	59	58	64[j]	47
	(11)	(47)	(12)	(13)	(44)	(11)	(11)	(58)	(11)	(11)	(11)	(34)	(5)
δ	112	112	113	114	112	112	111	118	111	110	116	114	137
	(19)	(19)	(20)	(19)	(18)	(18)	(21)	(20)	(25)	(25)	(25)	(25)	(8)
ε	189	189	190	189	188	189	189	195	190	203[f]	210[h]	205[k]	184
	(10)	(10)	(11)	(10)	(10)	(10)	(10)	(13)	(11)	(36)	(40)	(35)	(12)
ζ	271	271	272	271	271	271	273	276	273	244[g]	234[i]	249[l]	258
	(13)	(13)	(13)	(13)	(12)	(12)	(14)	(14)	(16)	(69)	(73)	(53)	(15)
χ	225	224	224	224	223	223	222	221	226	236	241	237	247
	(18)	(18)	(20)	(18)	(17)	(18)	(19)	(23)	(19)	(32)	(33)	(26)	(7)
P	116	117	119	115	117	116	112	123	111	108	120	115	154
	(31)	(35)	(40)	(31)	(32)	(30)	(48)	(32)	(59)	(65)	(55)	(60.0)	(17)

[a]γ in first nucleotide goes to *trans* region. [b]γ in first nucleotide goes to *trans* region. [c]α in 6th nucleotide oscillates between *trans*, and *gauche*$^-$ region. [d]β in 5th nucleotide adopts in g^+ region. [e]Some γ angles in 1st and 6th nucleotides adopt *trans* values. [f,g,h,i,k,l]ε and ζ angles in 1st nucleotide for 2nd, 3rd and 4th strand in PA structure adopt g^-, g^+ region values respectively. [j]γ angles in first and second nucleotides go to *trans* region.

The global helical parameters have also been calculated for the three quadruplex structures, taking the first two strands as a pair. It is observed that the negative inclination value (-1.4º) in PA structure is smallest among the three structures whereas average inclination value in PA-Na structure (-2.7º) is close to the average crystal structure value (-3.7º). PA-Na, PA-K and PA structures all have negative tip values (-2.0º, -2.9º and -2.7º respectively), while crystal structure has positive tip value (6.1º). Na^+ and K^+ ion coordinated structures exhibit mean twist values close to the crystal structure value (29.0º). However, in PA structure, after 300 ps of dynamics, twist value decreases without affecting the helical rise and stabilizes around 27.0∞. Average values for the translational parameters for the PA-Na and PA-K structures remain close to the crystal structure values while they show much deviation in the PA structure. Average 'dx' and 'dy' values in PA structure (-6.1Å and -0.5Å) are more negative than the average crystal structure values (-4.1Å and 0.0Å), as well as for the PA-Na and PA-K structures. However, 'rise' in all three structures are comparable with the crystal structure value (3.5Å). It is also observed that as in the case of backbone torsion angles, the structural parameters for PA structure also fluctuate more than those of PA-Na and PA-K structures.

The intra and inter basepair parameters as defined by the Cambridge convention (62) have been calculated for the MD average structures and the average values, over all six steps of the 7-mer quadruplex structures are listed in Table V. All the three MD average structures have small positive tilt and small negative propeller twist values whereas the crystal structure has small negative tilt and almost zero propeller twist. Base tetrads in MD average structures are less buckled than the crystal structure. Other rotational and translational parameters in the PA-Na, PA-K and PA structures are close to the crystal structure values. Most step parameters for the G-tetrads show only small variations in the ion coordinated structures, particularly for the middle segments. However, even these small base movements lead to the phosphate cylinder radius as well as C1' cylinder radius also becoming slightly larger in the K^+ ion coordinated structures as compared to the Na^+ ion coordinated structures. This occurs without affecting the groove width, as defined by the shortest P—P separation on neighbouring strands. This confirms our earlier deduction that the guanine quadruplexes accommodate different cations by rotating the guanine bases in the G-quartets rather than by their translation movement. The intra and inter basepair parameters in the PA structure show larger standard deviation, again indicating the greater flexibility of this structure. In addition, phosphate cylinder radius (r_p), C1′ cylinder radius ($r_{c1'}$) and groove width, as defined by the inter-strand P-P separation, all become larger for PA than in the sodium coordinated crystal structure and the MD average PA-Na structure, indicating that in the absence of coordinated ions, the four strands in the quadruplex have moved apart or stated differently, the coordinated cations hold the strands closer together.

Comparison of MD Results with Experimental Data

Several electrophoretic, NMR and CD spectroscopic studies have demonstrated (28-43) that in the presence of a Na^+ or K^+ ion, guanine rich sequences can form different type of quadruplexes, though an oligo d(G) sequence has only been crystallized with Na^+ ions coordinated within a parallel stranded (TG_4T) quadruplex. In order to compare the MD average PA-Na structure with the available Na^+ ion coordinated crystal structure, the 4-mer crystal structure, including the three coordinated ions is superimposed on the 3rd, 4th, 5th and 6th nucleotides of the 7-mer MD average PA-Na structure and shown in Figure 10A. When the same four nucleotides in the MD average PA-K and PA structures are super imposed on the crystal structure, it is observed that the rms deviation between the PA-Na and crystal structure, as well as, between PA-K and crystal structure are quite small (0.71Å and 0.89Å respectively), while the rms deviation between the PA structure and crystal structure is 1.19Å. Second G-tetrad of the crystal structure is also superimposed on middle (4th) tetrad of PA-Na structure and a down the axis view of super-

Table V

Average inter and intra basepair parameters, C1′ cylinder radius ($r_{C1'}$), phosphate cylinder radius (r_P) and groove width in the fibre model (18) and crystal structure (21) are listed along with the values for the various MD average 7-mer quadruplex structures. The parameters have been calculated taking the four strands pairwise and their standard deviation values are given within parentheses. Rotational parameters are in degrees and translational parameters are in Å unit.

	Fiber	Crystal	PA-Na	PA-K	PA
Tilt	-3.3	-2.7	1.0	1.5	1.9
	-	(1.3)	(1.4)	(1.0)	(3.1)
Roll	0.0	1.2	1.9	0.3	-0.4
	-	(2.5)	(1.6)	(1.9)	(6.5)
Local	31.1	29.7	29.2	29.1	27.1
Twist	-	(2.6)	(2.0)	(2.3)	(3.5)
Shift	-0.4	-0.5	0.1	0.2	0.3
	-	(0.8)	(0.2)	(0.2)	(0.5)
Slide	-2.5	-2.4	-2.2	-2.3	-2.4
	-	(0.3)	(0.2)	(0.2)	(0.5)
Rise	3.4	3.4	3.4	3.3	3.3
	-	(0.1)	(0.1)	(0.3)	(0.3)
Propeller	4.5	-1.3	-2.6	-2.5	-5.2
Twist	-	(4.1)	(2.2)	(2.0)	(9.5)
Buckle	11.7	-12.4	-3.1	-5.9	-5.4
	-	(3.7)	(6.6)	(2.7)	(11.9)
$r_{C1'}$	7.9	7.6	7.6	7.9	7.9
	-	(0.2)	(0.2)	(0.1)	(0.8)
r_P	10.9	11.0	11.1	11.4	11.4
	-	(0.4)	(0.1)	(0.1)	(0.7)
Groove width[a]	8.5	8.9	9.0	8.9	10.1
	-	(0.6)	(0.2)	(0.4)	(1.4)

[a]Groove width or shortest P---P separation on neighbouring strands corresponds to distance between phosphates separated by two guanine tetrads.

imposed G-tetrads is shown in the Figure 10B, which clearly indicates the differences in hydrogen bonding patterns in the middle G-tetrads of the two structures. Thus, it is seen that PA-Na, the MD average parallel quadruplex structure with coordinated sodium ions, is very similar to the G4 tract in this crystal structure (21), eventhough bifurcated hydrogen bonds are seen in the central three G-tetrads of the MD structure. In addition, the distance between the coordinated sodium ion and the O6 atoms of G-tetrads in the MD average PA-Na structure (~2.5Å) is shorter than the value observed in the crystal structure (~2.9Å). This is due to the minima in the Na^+—O6 interaction energy occurring at ~2.2Å in the AMBER force field (50) when the Aqvist (52) parameters are used for the ion. The total ion-guanine interaction energy is also found to be highly favourable with the AMBER force field. The Na^+ ion to O6 distance in the crystal structure is also seen to reduce from its original value after few cycles of minimization. It is observed that during the MD simulation, coordinated Na^+ ions in the PA-Na structure transiently occupy positions in-plane with the G-tetrad as well as outside the quadruplex channel, but subsequently return to the DNA core. This type of coordinated Na^+ ion movement, along the quadruplex axis is also observed in MD simulation of antiparallel Greek key type quadruplex (unpublished data). Movement of a Na^+ ion towards an in-plane location on the terminal G-quartet is also observed in the crystal structure as well as in several NMR studies (46-48). However, we do not observe a stable position for the Na^+ ion in the G-tetrad plane as reported in the crystal structure, indicating that an intercalated position between two G-tetrads is the most favoured location for an ion. Contrary to the large movements observed for the coordinated Na^+ ion, within the 1 ns MD simulations, the K^+ ions are quite immobile. These results are in agreement with NMR data (46-48) which indicates that residence time of a sodium ion within the quadruplex channel is smaller than that of a potassium ion and also association/dissociation studies on $d(TG_4)_4$ in the presence of K^+ ions, indicate that 3 to 5 potassium ions are tightly bound to the quadruplex and these ions are entrapped during the quadruplex formation itself (48).

Crystal structure (20) of the hairpin dimer, formed by the telomeric sequence $d(G_4T_4G_4)$, with K^+ ion shows distortion in base tetrads which results in several three centered or bifurcated hydrogen bonds within the G-tetrads. Several other structural parameters *e.g.* backbone torsion angles also show large variation. Our MD results also indicate that the bases in the G-tetrads of K^+ ion coordinated structures undergo in-plane rotation, leading to slightly different hydrogen bonding patterns in neighbouring tetrads as well as being different from that seen in the Na^+ ion coordinated structures, which could explain the differences observed between the NMR spectrum (42,44) of Na^+ and K^+ ion coordinated structures.

K^+ ion coordinated parallel quadruplexes were found to be slightly less favourable from enthalpy considerations, than the corresponding Na^+ ion coordinated structure. This is in agreement with free energy perturbation calculation (44) and thermodynamic studies (43) which have also demonstrated that a sodium ion binds the coordination sites of G-quadruplex with slightly more favourable free energy than a potassium ion. It was also suggested from the thermodynamic study that the higher desolvation energy of Na^+ over K^+ ion was responsible for the observed preference of K^+ ion for quadruplex formation, rather than a better fit for the K^+ ion within the cavity, as deduced from some earlier data (43). Our MD studies also indicate that a Na^+ ion is accommodated most readily within a G-quadruplex with minimal distortion of the G-tetrads. However, this ion is quite mobile within the central cavity and can be expelled more easily than the larger K^+ ion, thus accounting for the higher melting temperature observed for the K^+ ion coordinated quadruplex (32,40).

Conclusions

On the basis of our MD studies, it can be concluded that parallel G-quadruplexes are very stable structures, both energetically as well as structurally. Base interaction energy within the G-tetrad, as well as guanine tetrad stacking energy in PA structure, are more favourable than in PA-Na and PA-K structures. However, inclusion of the contribution due to the coordinated ion in energy calculations makes PA-Na and PA-K structures more favourable than the PA structure with water molecules in the central cavity. Base interaction energy within the G-tetrad primarily depends on O6 atom orientation and hydrogen bonding scheme within the G-tetrad. In-plane base rotation in the middle G-tetrads in the PA-Na and PA-K structures brings O6 atoms closer together while also distorting the hydrogen bonds and consequently, base interaction energies in middle G-tetrads are less favourable than the terminal tetrads, which show standard Hoogsteen type hydrogen bonds. In the absence of any coordinated ion, due to O6—O6 repulsion, adjacent guanine bases in the PA structure rotate in opposite direction to that found in the PA-K structure, leading to additional N2-H2$\cdots$O6 hydrogen bonds and more favourable base-base interaction energy within the G-tetrads.

Quadruplex structures with coordinated ions (Na^+ or K^+) are less flexible than the quadruplex with water molecules in the cavity. In contrast to the recently reported MD studies on 4-mer quadruplexes (27), we find that the 7-mer quadruplex structure with waters in the cavity remains intact during the simulation. In this structure, the central cavity is occupied by water molecules, during the heating phase itself, but subsequently one Na^+ ion from the solvent also enters through the 3′-end of the pre-formed quadruplex and coordinates with O6 atoms of the two terminal G-tetrads. Analysis of the 7-mer PA and PA-Na structures clearly shows that Na^+ ions can enter and exit through the quadruplex ends within our molecular dynamics time scale, while coordinated K^+ ions are static within their respective coordination sites.

Na^+ counter ions in the solvent bind most often to the phosphate groups, in all the three structures. However, a few counter ions are also located within the quadruplex grooves. In all the three structures, several hydrogen bonded water molecules are observed within the shallow quadruplex grooves. Water molecules are localized

around the exposed 2-amino group and N3 atom of guanine bases in the G-tetrads. A few of the exposed N7 atoms in the PA structure also act as good binding sites for water molecules.

In conclusion, the G-quadruplex is a very stable structure, which can undergo small variations in the G-tetrad geometry, depending on the presence of ions or solvent molecules in the central cavity, while retaining its overall structural integrity. The slightly shorter ion—O6 distances observed in the Na^+ ion coordinated MD structures (25,27), as compared to the high-resolution crystal structure, probably suggests that the ion parameters need further refinement.

Acknowledgement

This work is partially supported by a grant from CSIR, INDIA. The authors are grateful to SERC, I. I. Sc., for computational facilities.

References and Footnotes

1. M. Gellert, M.N. Lipsett and D.R. Davies, *Proc. Natl. Acad. Sci. U.S.A. 48*, 2013-2018 (1962).
2. W. Guschlbauer, J.F. Chantot and D. Thiele, *J. Biomol. Struct. Dyn. 8*, 491-511 (1990).
3. T.R. Cech, *Nature 332*, 777-778 (1988).
4. W.I. Sundquist and A. Klug, *Nature 342*, 825-829 (1989).
5. J.R. Williamson, M.K. Raghuraman and T.R. Cech, *Cell 59*, 871-880 (1989).
6. E. Blackburn, *Nature 350*, 569-573 (1991).
7. D. Sen and W. Gilbert, *Nature 334*, 364-366 (1988).
8. A.I.H. Murchie and D.M.J. Lilley, *Nucl. Acids Res. 20*, 49-53 (1992).
9. K. Walsh and A. Gualberto, *J. Biol. Chem. 267*, 13714-13718 (1992).
10. W.I. Sundquist and S. Heaphy, *Proc. Natl. Acad. Sci. U.S.A. 90*, 3393-3397 (1993).
11. A. Kettani, R.A. Kumar and D.J. Patel, *J. Mol. Biol. 254*, 638-656 (1995).
12. J.R. Williamson, *Curr. Opin. Struct. Biol. 3*, 357-362 (1993).
13. J.R. Williamson, *Annu. Rev. Biophys. Biomol. Struc. 23*, 703-730 (1994).
14. G. Fang and T.R. Cech, *Biochemistry 32*, 11646-11657 (1993).
15. P.W. Shomer and M. Fry, *J. Biol. Chem. 268*, 3306-3312 (1993).
16. K.Y. Wang, S.H. Krawczyk, N. Bischofberger, S. Swaminathan and P.H. Bolton, *Biochemistry 32*, 11285-11292 (1993).
17. R. Giraldo and D. Rhodes, *EMBO J. 13*, 2411-2420 (1994).
18. S. Arnott, R. Chandrasekaran and C.M. Marttila, *Biochem. J. 141*, 537-543 (1974).
19. S.B. Zimmerman, G.H. Cohen and D.R. Davies, *J. Mol. Biol. 92*, 181-192 (1975).
20. C. Kang, X. Zhang, R. Ratliff, R. Moyzis and A. Rich, *Nature 356*, 126-131 (1992).
21. K. Phillips, Z. Dauter, A.I.H. Murchie, D.M.J. Lilley and B. Luisi, *J. Mol. Biol. 273*, 171-182 (1997).
22. D. Mohanty and M. Bansal, *Nucl. Acids Res. 21*, 1767-1774 (1993).
23. D. Mohanty and M. Bansal, *Biopolymers 34*, 1187-1211 (1994).
24. D. Mohanty and M. Bansal, *Biophys. J. 69*, 1046-1067 (1995).
25. M. Bansal, M. Ravikiran and S. Chowdhury, *Computational Molecular Biology* (edited by J. Leszczynski), *Elsevier Science*, 279-323 (1999).
26. J. Gu, J. Leszczynski and M. Bansal, *Chem. Phys. Letters 311*, 209-214 (1999).
27. N. Spackova, I. Berger and J. Sponer, *J. Am. Chem. Soc. 121*, 5519-5534 (1999) .
28. P. Balagurumoorthy, S.K. Brahmachari, D. Mohanty, M. Bansal and V. Sasisekharan, *Nucl. Acids Res. 20*, 4061-4067 (1992).
29. J. Kim, C. Cheong and P.B. Moore, *Nature 351*, 331-332 (1991).
30. F. Aboul-ela, A.I.H. Murchie and D.M.J. Lilley, *Nature 360*, 280-282 (1992).
31. Y. Wang and D.J. Patel, *J. Mol. Biol. 234*, 1171-1183 (1993).
32. C.C. Hardin, E. Henderson, T. Watson and J.K. Prosser, *Biochemistry 30*, 4460-4472 (1991).
33. C.C. Hardin, T. Watson, M. Corregan and C. Bailey, *Biochemistry 31*, 833-841 (1992).
34. T. Miura and G.J. Thomas Jr, *Biochemistry 34*, 9645-9654 (1995).
35. G. Gupta, A.E. Garcia, Q. Guo, M. Lu and N.R. Kallenbach, *Biochemistry 32*, 7098-7103 (1993).
36. Y. Wang, C.D. L. Santos, X. Gao, K. Greene, D. Live and D.J. Patel, *J. Mol. Biol. 222*, 819-832 (1991).
37. F.W. Smith and J. Feigon, *Nature 356*, 164-168 (1992).
38. P. Schultze, R.F. Macaya, F.W. Smith, J.A. Roe and J. Feigon, *Proc. Natl. Acad. Sci. U.S.A. 90*, 3745-3749 (1993).
39. K. Padmanabhan, K.P. Padmanabhan, J.D. Ferrara, J.E. Sadler and A. Tulinsky, *J. Biol. Chem. 268*, 17651-17654 (1993).
40. P. Balagurumoorthy and S. K. Brahmachari, *J. Biol. Chem. 269*, 21858-21869 (1994).
41. D. Sen and W. Glibert, *Nature 344*, 410-414 (1990).

42. T. Miura, J.M. Benevides and G.J. Thomas Jr, *J. Mol. Biol*. *248*, 233-238 (1995).
43. N.V. Hud, F.W. Smith, F.A.L. Anet and J. Feigon, *Biochemistry 35*, 15383-15390 (1996).
44. W.S. Ross and C.C. Hardin, *J. Am. Chem. Soc. 116*, 6070-6080 (1994).
45. P.V. Scaria, S.J. Shire and R.H. Shafer, *Proc. Natl. Acad. Sci. U.S.A. 89*, 10336-10340 (1992).
46. Q. Xu, H. Deng and W.H. Braunlin, *Biochemistry 32*, 13130-13137 (1993).
47. H. Deng and W.H. Braunlin, *J. Mol. Biol. 255*, 476-483 (1996).
48. C.C. Hardin, M.J. Corregan, D.V. Lieberman and B.A. Brown II, *Biochemistry 36*, 15428-15450 (1997).
49. N.V. Hud, P. Schultze, V. Sklenar and J. Feigon, *J. Mol. Biol*. *285*, 233-243 (1999).
50. W.D. Cornell, P. Cieplak, C.I. Bayly, I.R. Gould, K.M. Merz Jr., D.M. Ferguson, D.C. Spellmeyer, T. Fox, J.W. Caldwell and P.A. Kollman, *J. Am. Chem. Soc*. *117*, 5179-5197 (1995).
51. T. Darden, D. York and L. Pedersen, *J. Chem. Phys. 98*, 10089-10092 (1993).
52. J. Aqvist, *J. Phys. Chem. 94*, 8021-8024 (1990).
53. M.A. Young, G. Ravishankar and D.L. Beveridge, *Biophys. J.* 73, 2313-2336 (1997).
54. Y. Duan, P. Wilkosz, M. Crowley and J.M. Rosenberg, *J. Mol. Biol. 272*, 553-572 (1997).
55. M. Feig and B.M. Pettitt, *Biophys. J. 77*, 1769-1781 (1999).
56. T.E. Cheatham III, P. Cieplak and P.A. Kollman, *J. Biomol. Struct. Dyn. 16*, 845-862 (1999).
57. M. Feig and B.M. Pettitt, *Biophys. J. 75*, 134-149 (1998).
58. D. Bhattacharyya and M. Bansal, *J. Biomol. Struct. Dyn. 6*, 635-653 (1989).
59. M. Bansal, D. Bhattacharyya and B. Ravi, *CABIOS 11*, 281-287 (1995).
60. S. Weerasinghe, P.E. Smith, V. Mohan, Y.K. Cheng and B.M. Pettitt, *J. Am. Chem. Soc*. *117*, 2147-2158 (1995).
61. B. Schneider, D. M. Cohen, L. Schleifer, A. R. Srinivasan, W. K. Olson and H. M. Berman, *Biophys. J. 65*, 2291-2303 (1993).
62. R.E. Dickerson *et al*, *J. Mol. Biol 205*, 787-791 (1989).

Date Received: April 6, 2000

Communicated by the Editor Wolfram Saenger